SCIENCE CHINA
Information Sciences

• RESEARCH PAPER •

June 2022, Vol. 65 162403:1–162403:7
https://doi.org/10.1007/s11432-021-3331-3

Second harmonic generation in a hollow-core fiber filled with GaSe nanosheets

Zhen HAO, Yuxin MA, Biqiang JIANG*, Yueguo HOU, Ailun LI, Ruixuan YI, Xuetao GAN* & Jianlin ZHAO

MOE Key Laboratory of Material Physics and Chemistry Under Extraordinary Conditions and Shaanxi Key Laboratory of Optical Information Technology, School of Physical Science and Technology, Northwestern Polytechnical University, Xi'an 710129, China

Received 18 May 2021/Revised 13 July 2021/Accepted 5 September 2021/Published online 12 April 2022

Abstract Frequency conversions using various all-fiber nonlinear devices can benefit many applications, including communications, sensing, microscope, and imaging. In this study, we report in-fiber second harmonic generation (SHG) in an optical hollow-core fiber (HCF) that can be used for frequency conversion. The HCF filled with a dispersion of gallium selenide (GaSe) nanosheets in the ultraviolet-cured optical adhesive supports a well-propagating mode in the fiber core, which enables effective light interaction with dispersed GaSe nanosheets and a strong SHG process. Based on theoretical analysis, the optimal HCF length for maximizing SHG is approximately 0.41 mm. The broadband SHG of the GaSe-filled HCF device is demonstrated by tuning the pump wavelength from 1460 to 1600 nm. Moreover, a time-varied SHG in the device is revealed due to additional second-order susceptibility induced by the polarization of silica. The proposed device with a compact and robust structure has the potential to be connected to existing all-fiber telecom and sensing systems for numerous nonlinear engineering applications.

Keywords second-harmonic generation, gallium selenide, hollow-core fiber, broadband operation wavelength, time-varied second harmonic generation

Citation Hao Z, Ma Y X, Jiang B Q, et al. Second harmonic generation in a hollow-core fiber filled with GaSe nanosheets. Sci China Inf Sci, 2022, 65(6): 162403, https://doi.org/10.1007/s11432-021-3331-3

1 Introduction

So far, a pristine optical fiber was seldom used in frequency conversion based on second-order nonlinear processes, such as the second harmonic generation (SHG) and sum-frequency generation, due to the centrosymmetry of fused silica [1], although weak surface SHGs could be observed due to the break of centrosymmetry at the core-cladding interface [2], which hinders the implementations of nonlinear all-fiber devices based on second-order nonlinear processes. Thus, various fiber postprocesses, such as optical poling [3], thermal poling [4], and electric field poling [5], have been performed to break silica fiber's inversion symmetry. However, these methods require complex operations, thereby leading to increased costs, low device reliability, and low production yield. Recently, we have excited SHG using gallium selenide (GaSe) nanoflakes integrated with microfibers with a wide operating wavelength range covering O, C, and L bands [6]. Nevertheless, a delicate microfiber with GaSe nanosheets exposed to air is easily susceptible to environmental disturbances, such as vibrations, dust capture, and oxygenization. Therefore, achieving the SHG in a wide wavelength range with a robust structure will still be appealing.

In this article, we report a hollow-core fiber (HCF) filled with GaSe nanosheets to implement strong SHG with high reliability and stability. The lack of centrosymmetry endows GaSe with high second-order nonlinear susceptibility $\chi^{(2)}$ [7], and this material with a moderate laser damage threshold [8] is an ideal option for second-order nonlinear processes [6]. With the advantages of nonresonant excitation and strong light-matter interaction, we observed SHG from a GaSe-filled HCF device in the wavelength range of 1460–1600 nm and at 1064 nm, implying a broadband operation wavelength range. In addition,

* Corresponding author (email: bqjiang@nwpu.edu.cn, xuetaogan@nwpu.edu.cn)

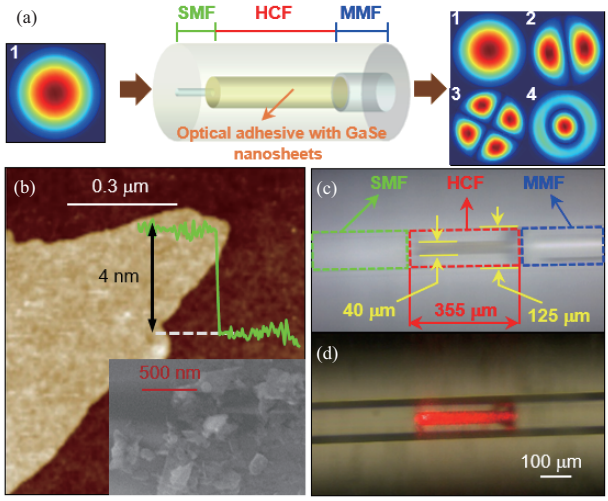

Figure 1 (Color online) (a) Schematic of HCF device and the input fundamental mode 1 $LP_{01}(\omega)$ and output modes 1–4, including $LP_{01}(\omega)$, $LP_{11}(2\omega)$, $LP_{21}(2\omega)$, and $LP_{02}(2\omega)$. (b) Characterizations of a large GaSe nanosheet using an atomic force microscope and stacked GaSe nanosheets using a scanning electron microscope. (c) and (d) Optical microscopic images of the GaSe-filled HCF device under bright and dark fields, respectively.

the SHG intensity produced by the HCF device depends on pump illumination time, which is attributed to periodic $\chi_{\mathrm{p}}^{(2)}(2\omega = \omega + \omega)$ generated by second- and third-order nonlinear processes of an MMF through the HCF device. Considering the popularity of the fiber system [9–11], the proposed all-fiber frequency generator assisted by layered GaSe nanosheets may provide a method for developing broadband nonlinear fiber devices based on the second-order nonlinearity, such as new laser sources and all-optical signal processing. Moreover, the HCF device exhibits self-enhanced SHG intensity induced by the second- and third-order nonlinear processes, which provide another flexibility for realizing enhanced SHG based on this mechanism.

2 Device design and characterizations

2.1 Device fabrication and characterizations

Figure 1(a) depicts the structure of the HCF device. To assist the light coupling and propagation, an SMF and an MMF are connected with the HCF, as shown in green, red, and blue regions. A hollow quartz tube with an inner diameter of 127 μm was used to wrap the three regions. The inner and outer diameters of HCF are 40 and 125 μm, respectively, making it convenient to connect with SMF and MMF. As depicted in Figure 1(a), the optical adhesive with GaSe nanosheets is filled into the HCF to form a stable waveguide structure, supporting multimode propagation of the pump light and SHG due to the relatively large inner diameter. The phase-match condition can be well-satisfied between $LP_{01}(\omega)$ and $LP_{11}(2\omega)$, $LP_{21}(2\omega)$, and $LP_{02}(2\omega)$ with their mode profiles shown in Figure 1(a) and numbered 1–4, respectively. According to the theoretical calculation, the phase-mismatch parameter $\Delta\beta_{\mathrm{SHG}} = 2\beta(\omega) - \beta(2\omega)$ between the pump fundamental mode and the three SHG modes is quite small [12], with the magnitude of 10^{-4} rad/μm, and a long nonlinear interaction length is feasible before dephasing between the fundamental and SHG modes. Notably, other high-order SHG modes were not considered due to relatively large effective refractive index (RI) differences with the pump fundamental mode and extremely low mode conversion.

In the HCF device fabrication process, GaSe was selected as the nonlinear material. Owing to the nonresonant pump, the transparency of GaSe nanosheets was high in 0.7–18.0 μm wavelength range [13], making it a reliable material for exciting SHG in a wide range. The ε-GaSe with the AA stacking sequence leads to the absence of an inversion center for an arbitrary layer, which can be fabricated by chemical vapor deposition. As a consequence of the D_{3h} point group of ε-GaSe nanosheets [7], the only nonzero element d_{22} in second-order nonlinear susceptibility tensor $\chi^{(2)}$ was 180 pm/V, which was seven times that of the widely used $LiNbO_3$ crystal [14, 15], enabling considerable SHG. To obtain the thickness of the GaSe nanosheets, we characterized a relatively large GaSe nanosheet by an atomic force microscope.

From Figure 1(b), the thickness of a GaSe nanosheet was ∼4 nm, corresponding to five layers with a monolayer thickness of ∼0.83 nm [6,7]. Besides, the size of GaSe nanosheets used in the device fabrication processes ranges from 0.05 to 1 μm, which are characterized in the inset of Figure 1(b) using a scanning electron microscope.

Based on the capillarity phenomenon [16], the HCF core was filled with a mixture of GaSe nanosheets and the ultraviolet-cured optical adhesive (∼0.3 mg/μL), and then the mixture was cured under the illumination of a ∼375 nm light source. Finally, we filled 80% glycerol, whose RI was approximate to that of silica, into the gaps among SMF, HCF, and MMF to eliminate their optical interfaces. The RI of the cured optical adhesive was ∼1.56, which was higher than that of HCF, indicating that a stable waveguide was fabricated (Figure 1(c)). This HCF device with inner-filled GaSe nanosheets is immune to oxidation [17] and dust absorption, enabling long-term stability of the SHG excitation. From Figure 1(d), the GaSe nanosheets scattered red light when a 655 nm red-light source was launched from the SMF of the HCF device.

2.2 Selection of the hollow-core fiber length

For the device design, the HCF length was required to be optimized for maximum SHG intensity. The scattering loss and generation of SHG were simultaneously considered, wherein the quite small absorption coefficient 0.3 cm^{-1} of GaSe was negligible [13]. The quadratic-dependence of SHG intensity $I(2\omega)$ on pump light intensity $I(\omega)$ and HCF length L can be expressed as follows [18]:

$$I(2\omega) = I^2(\omega)|\rho|^2 L^2 \mathrm{sinc}^2(\Delta\beta_{\mathrm{SHG}} L/2), \tag{1}$$

where the nonlinear coupling parameter $\rho \propto \int \boldsymbol{P}^{(2)}(2\omega)\cdot\boldsymbol{e}(2\omega)\mathrm{d}S$ is determined by the coupling of second-order polarization to SHG modes in which $\boldsymbol{e}(2\omega)$ and $\boldsymbol{P}^{(2)}(2\omega)$ express the normalized electric field vectorial profiles of SHG modes and normalized amplitude vector of nonlinear polarization, respectively [18]. Notably, the integration was performed in an infinite plane that includes the HCF cross-section. To explore the optimal length of HCF corresponding to maximum SHG intensity, we initially fabricated a device with an HCF length of 1.1 mm. The transmission of the HCF device without filling GaSe nanosheets was simulated as 31%; then, according to the calibration results between the input and output power from the fabricated device, the loss factor α was calculated as 2.5 mm^{-1}, most of which must be the contribution of scattering loss of GaSe nanosheets. Assuming perfect phase-match and setting ρ as an arbitrary constant, we differentiated (1) with respect to L to obtain $\mathrm{d}I_{2\omega}(L)/\mathrm{d}L = 2L(1-\alpha L)[I_\omega(0)\mathrm{e}^{-\alpha L}]^2$. Subsequently, with the assistance of $I(L) = I(0)\mathrm{e}^{-\alpha L}$, which can be applied to both pump light and SHG, we calculated the dependences of pump and SHG intensities on HCF length (Figure 2). The intensities of the pump light and SHG had been normalized with respect to their maximum values. Intuitively, owing to the scattering loss and conversion to SHG, the pump light intensity always declined exponentially with HCF length L. However, the SHG intensity increased with L due to the conversion of the pump light energy to SHG and then decreased when the scattering loss dominated the frequency-conversion process. Specifically, the SHG intensity approximately increased quadratically when L was relatively small (inset of Figure 2), where the green curve represents the quadratic dependence. Nevertheless, when L was sufficiently large, owing to the scattering loss, the SHG intensity decreased almost exponentially with L. Consequently, the SHG exhibited a maximum intensity at 0.41 mm, and we defined an acceptable range (0.24–0.62 mm) and marked it as faint yellow in Figure 2, corresponding to above 80% maximum SHG intensities. In practical fabrication, limited by the optical fiber cleaver structure and the difficulty in manual operation, we fabricated the HCF as ∼0.36 mm, whereas the corresponding SHG intensity was almost the same as the calculated maximum.

3 Experimental arrangement and results

The experimental arrangement for measuring SHG is illustrated in Figure 3. The pump light from a picosecond laser propagated along the SMF and then intensely interacted with GaSe nanosheets in the HCF. To separate the SHG from the pump light, a collimating and filtering system comprising two collimators, a dichroic mirror, and a reflector was configured to filter out the pump light. A segment of MMF was used to realize the maximum collection efficiency of the SHG signal. Then, the SHG intensity was monitored in real-time using a spectrometer.

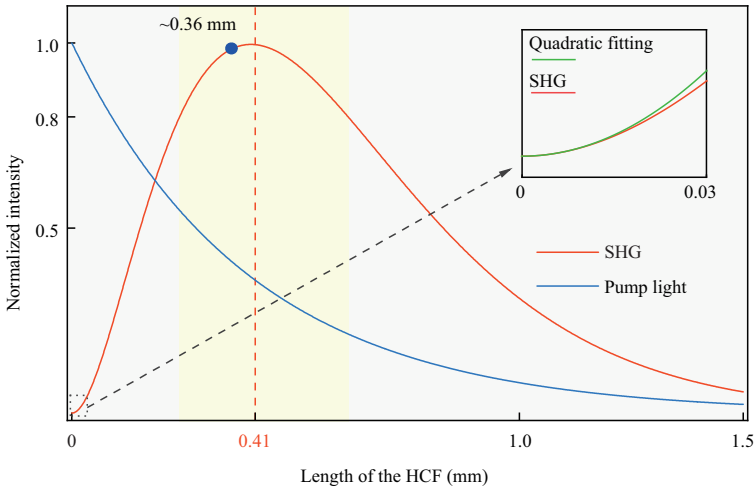

Figure 2 (Color online) Dependence relationships of SHG and pump laser intensities on the length of HCF. The orange and green curves in the inset represent the evolution of the SHG intensities with the length within 0.03 mm when the loss is considered or not, respectively.

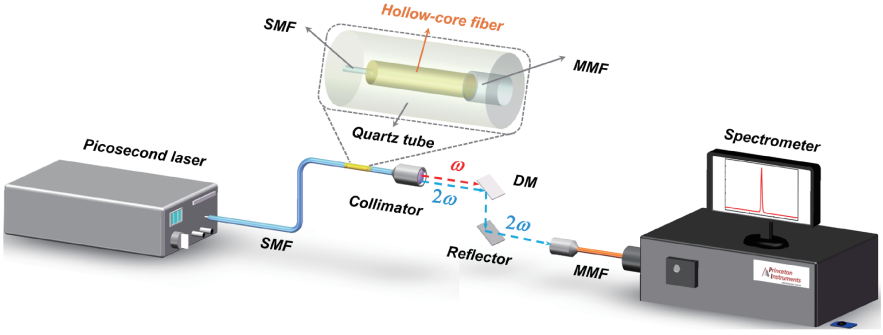

Figure 3 (Color online) Experimental arrangement for exciting and measuring second harmonic generation. DM: dichroic mirror.

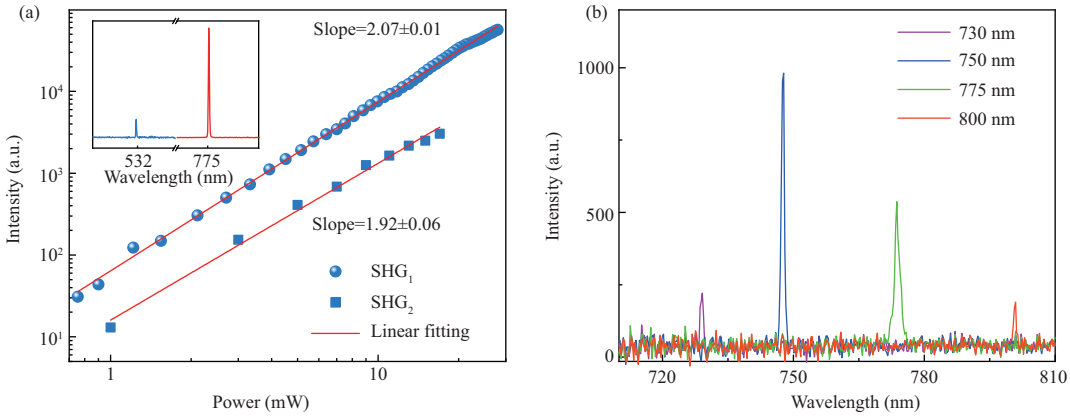

Figure 4 (Color online) (a) Log-log plot of SHG intensities at 775 and 532 nm; (b) broadband tuning of SHG when the pump wavelength ranges from 1460 to 1600 nm.

3.1 Power-dependence and broadband tuning of second harmonic generation

Considering a 1550-nm picosecond laser with 8.8 ps pulse width and a 18.5 MHz repetition rate to independently implement the SHG as an example, the power-dependence of the SHG at 775 nm (labeled SHG_1) was examined by modulating the pump power. The result is log-log plotted in Figure 4(a), showing a fitting slope of 2.07±0.01 in the entire power range. It agreed well with the prediction value 2 in (1).

Besides, the waveguide chromatic dispersion was weak due to the relatively large diameter (40 μm) of

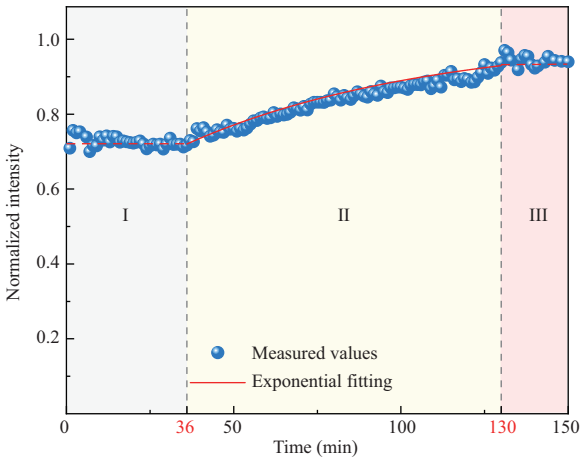

Figure 5 (Color online) Additional $\chi_{\mathrm{P}}^{(2)}$ grating enhanced second harmonic generation with pump time, including three parts: initial preparation-stage I, growth-stage II, and saturation-stage III.

the HCF, meaning that effective RIs of phase-matched modes would slightly evolve with pump wavelength, which approximately enables a relaxed phase-match condition in a wide wavelength range. Therefore, the device can be tailorable for a broadband wavelength operation. To verify this, far away from 1550 nm, a laser at 1064 nm supplied by another picosecond laser with 11 ps pulse width and a 19.5 MHz repetition rate was applied to excite the SHG at 532 nm (labeled SHG_2). The results are shown in Figure 4(a). As the pump power increased, the slope 1.92±0.06 of power-dependence also approached the theoretical value 2. However, from the spectra of SHG_1 and SHG_2 at two wavelengths in the inset of Figure 4(a) and the curves of power-dependences, the intensity of the SHG_1 clearly exceeded that of SHG_2. This observation could be attributed to mechanisms that contain mainly absorption at short wavelength regions below 700 nm induced by GaSe nanosheets but also likely that of silica [19]. Moreover, the dependence of SHG at more available pump wavelengths ranging from 1460 to 1600 nm was investigated and is shown in Figure 4(b), by replacing the picosecond laser in Figure 3 with a widely tunable picosecond optical parameter oscillator (OPO). The varied OPO output power with wavelength, modal interference, and wavelength-dependent phase-mismatch parameter caused obvious fluctuations in the SHG intensity during wavelength scanning. Still, the broadband character of the GaSe-filled HCF device was demonstrated for the excitation of second-order nonlinear processes.

3.2 Additional $\chi_{\mathrm{P}}^{(2)}$ grating enhanced second harmonic generation intensity

To assess the SHG output stability of the HCF device, we characterized the SHG intensity continuously for 150 min, and a ∼1.29 times' enhancement was observed, which could be ascribed to the poled MMF after the HCF device. With the 1550 nm laser as the pump laser, the applied experimental setups were the same as that illustrated in Figure 3. The evolution of the SHG intensity could be divided into three parts: initial preparation-stage I, growth-stage II and saturation-stage III. For region I corresponding to 0–36 min in Figure 5, only slight fluctuations in the SHG intensity were observed. However, for the exponential growth stage of region II from 36 to 130 min, the SHG intensity almost grew exponentially with the pump illumination time [20, 21] and reached the maximum value at 130 min. After 130 min in region III, the SHG intensity saturated and stopped growing.

These interesting observations, including self-enhanced SHG in growth-stage II and plateaued SHG maximum intensity in saturation-stage III, could be ascribed to the second- and third-order nonlinear processes of silica fiber [22]. For the growth-stage II, the gradually developed second-order nonlinear susceptibility $\chi_{\mathrm{P}}^{(2)}(2\omega = \omega + \omega)$, which periodically distributed along the successive MMF after the HCF device, leading to a growing SHG, was also observed in a previous report [23]. Specifically, analogous to the usual second-order optical rectification, a direct-current (DC) polarization P_{DC} was induced, which originated from the third-order nonlinear susceptibility $\chi^{(3)}(0 = -2\omega + \omega + \omega)$ of the silica fiber (MMF) after the GaSe-filled HCF device, as shown in (2) [22]:

$$P_{\mathrm{DC}} = (3\epsilon_0/4)\mathrm{Re}[\chi^{(3)} E_{2\omega} E_{\omega}^{*} E_{\omega}^{*} \exp(\mathrm{i}\Delta\beta_{\mathrm{DC}} z)], \tag{2}$$

where the pump light and SHG excited by GaSe nanosheets contributed to E_{ω}^{*} and $E_{2\omega}$, respectively, and the z-axis is the axis of the optical fibers. The phase-mismatch parameter is $\Delta\beta_{\mathrm{DC}} = \beta(2\omega) - \beta(\omega) - \beta(\omega)$, where $\beta(\omega)$ and $\beta(2\omega)$ represent the propagation constants of the fundamental and high-order modes of the SHG, respectively. Considering the contribution to the formation of the periodic $\chi_{\mathrm{P}}^{(2)}(2\omega = \omega + \omega)$, SHG excited by GaSe nanosheets was called the seed second harmonic generation (SSHG). The DC polarization P_{DC} would create a DC electric field E_{DC} whose polarity changed with the fiber with a $2\pi/\Delta\beta_{\mathrm{DC}}$ phase-match period. The DC electric field E_{DC} will redistribute the electric charges and break the inversion symmetry in the silica. According to the relation $\chi_{\mathrm{P}}^{(2)} = \gamma P_{\mathrm{DC}}$, the periodic $\chi_{\mathrm{P}}^{(2)}(2\omega = \omega + \omega)$ was generated along the HCF device, where γ is a constant characterizing the magnitude of the $\chi_{\mathrm{P}}^{(2)}(2\omega = \omega + \omega)$. After 130 min, the SHG intensity saturated due to the SHG generated by the periodic $\chi_{\mathrm{P}}^{(2)}(2\omega = \omega + \omega)$ induced an additional $\chi_{\mathrm{ad}}^{(2)}(2\omega = \omega + \omega)$, which was $\pi/2$ out of phase with the periodic $\chi_{\mathrm{P}}^{(2)}(2\omega = \omega + \omega)$. The additional $\chi_{\mathrm{ad}}^{(2)}(2\omega = \omega + \omega)$ also corresponded to a DC electric field $E_{\mathrm{DC}}^{'}$. When the electric field $E_{\mathrm{DC}}^{'}$ was comparable to E_{DC}, the periodic redistribution process of charges ceased, leading to the saturated SHG [22]. Notably, the magnitude of the periodic $\chi_{\mathrm{P}}^{(2)}(2\omega = \omega + \omega)$ relied on both the intensity of SSHG excited by GaSe nanosheets and the pump power. Therefore, additional grown SHG in a couple of hours could be due to the polarization of successive MMF, and then the total SHG intensity was contributed by the GaSe nanosheets and the SSHG-induced SHG in MMF. Provided no SSHG was produced by GaSe nanosheets, the total SHG intensity would remain constant even after a 12-h pump [22]. This indicated that, under the same pump power, the total saturated SHG intensity would increase markedly and more quickly if we replaced GaSe with other distinguished second-order nonlinear materials such as tellurium (Te) nanowire with $d_{11} = 650$ pm/V [24], providing a possibility of an HCF device filled with various nonlinear materials in practical applications.

4 Conclusion

In summary, we demonstrated an efficient SHG from a GaSe-filled HCF. By optimizing the HCF length based on the theoretical calculation, we obtained strong SHG with the assistance of GaSe nanosheets. Investigations on the power-dependence and broadband tuning of SHG indicate that the GaSe-filled HCF device can not only produce SHG under sub-milliwatt average power's pump but also possess an operation wavelength range over 100 nm, which could be enlarged to longer wavelengths due to the negligible absorption coefficient when $\lambda > 0.7$ μm [13]. Further studies on the stability of the device in 150 min pump illumination time revealed ∼1.29 times enhanced SHG due to the second- and third-order nonlinear processes in silica. Therefore, the proposed HCF frequency converter in an all-fiber structure can be developed for high-performance engineering applications and then merged with other nonlinear devices using fiber telecom systems.

Acknowledgements This work was supported by National Natural Science Foundation of China (Grant Nos. 61775182, 61975166, 61775183), Natural Science Basic Research Plan in Shaanxi Province of China (Grant No. 2019JM-330), and Fundamental Research Funds for the Central Universities. We also thank the Analytical & Testing Center of NPU for their assistance with the material and device characterizations.

References

1 Fujii Y, Kawasaki B S, Hill K O, et al. Sum-frequency light generation in optical fibers. Opt Lett, 1980, 5: 48–50
2 Javůrek D, Peřina J J. Analytical model of surface second-harmonic generation. Sci Rep, 2019, 9: 4679
3 Tombelaine V, Buy-Lesvigne C, Leproux P, et al. Optical poling in germanium-doped microstructured optical fiber for visible supercontinuum generation. Opt Lett, 2008, 33: 2011
4 Pruneri V, Samoggia F, Bonfrate G, et al. Thermal poling of silica in air and under vacuum: the influence of charge transport on second harmonic generation. Appl Phys Lett, 1999, 74: 2423–2425
5 Feng T L, Raabe N, Rustige P, et al. Electric-field induced second-harmonic generation of femtosecond pulses in atmospheric air. Appl Phys Lett, 2018, 112: 241101
6 Jiang B Q, Hao Z, Ji Y F, et al. High-efficiency second-order nonlinear processes in an optical microfibre assisted by few-layer GaSe. Light Sci Appl, 2020, 9: 63
7 Zhou X, Cheng J X, Zhou Y B, et al. Strong second-harmonic generation in atomic layered GaSe. J Am Chem Soc, 2015, 137: 7994–7997
8 Fernelius N C. Properties of gallium selenide single crystal. Prog Cryst Growth Charact Mater, 1994, 28: 275–353
9 Liu Z J, Jin X X, Su R T, et al. Development status of high power fiber lasers and their coherent beam combination. Sci China Inf Sci, 2019, 62: 041301
10 Dai W C, Lu Y, Zhu J, et al. An integrated quantum secure communication system. Sci China Inf Sci, 2011, 54: 2578–2591
11 Zhao D Y, Long K P, Zheng Y C, et al. Channel power control in optical amplifiers to mitigate physical impairment in optical network. Sci China Inf Sci, 2015, 58: 102305
12 Boyd R. Nonlinear Optics. 3rd ed. Pittsburgh: Academic Press, 2010

13 Allakhverdiev K R, Yetis M, Özbek S, et al. Effective nonlinear GaSe crystal. Optical properties and applications. Laser Phys, 2009, 19: 1092–1104
14 Bringuier E, Bourdon A, Piccioli N, et al. Optical second-harmonic generation in lossy media: application to GaSe and InSe. Phys Rev B, 1994, 49: 16971–16982
15 Xue D F, Zhang S Y. Comparison of non-linear optical susceptibilities of $KNbO_3$ and $LiNbO_3$. J Phys Chem Solids, 1997, 58: 1399–1402
16 Han A P, Mondin G, Hegelbach N G, et al. Filling kinetics of liquids in nanochannels as narrow as 27 nm by capillary force. J Colloid Interface Sci, 2006, 293: 151–157
17 Beechem T E, Kowalski B M, Brumbach M T, et al. Oxidation of ultrathin GaSe. Appl Phys Lett, 2015, 107: 173103
18 Hao Z, Jiang B Q, Hou Y G, et al. Continuous-wave pumped frequency upconversions in an InSe-integrated microfiber. Opt Lett, 2021, 46: 733
19 Akhundov G A, Gasanova N A, Nizametdinova M A. Optical absorption, reflection, and dispersion of GaS and GaSe layer crystals. Phys Stat Sol (b), 1966, 15: 109–113
20 Österberg U, Margulis W. Dye laser pumped by Nd:YAG laser pulses frequency doubled in a glass optical fiber. Opt Lett, 1986, 11: 516–518
21 Österberg U, Margulis W. Experimental studies on efficient frequency doubling in glass optical fibers. Opt Lett, 1987, 12: 57–59
22 Stolen R H, Tom H W K. Self-organized phase-matched harmonic generation in optical fibers. Opt Lett, 1987, 12: 585–587
23 Ceoldo D, Krupa K, Tonello A, et al. Second harmonic generation in multimode graded-index fibers: spatial beam cleaning and multiple harmonic sideband generation. Opt Lett, 2017, 42: 971
24 Sutherland R. Handbook of Nonlinear Optics. 2nd ed. Boca Raton: CRC Press, 2003